Chemical Physics 513 (2018) 241–245

Contents lists available at ScienceDirect

Chemical Physics

journal homepage: www.elsevier.com/locate/chemphys

The photocathodic properties of a Fe_2O_3 wrapped $CuFeO_2$ layer on ITO glass for water splitting

Xiaorong Cheng[a,*], Jianming Ding[b], Yangjiang Wu[a], Hao Liu[a], Graham Dawson[c,*]

[a] Suzhou Vocational Institute of Industrial Technology, Suzhou, Jiangsu 215104, PR China
[b] Jiangsu Key Laboratory of Thin Films and Department of Physics, Soochow University, Suzhou, Jiangsu 215006, PR China
[c] Department of Chemistry, Xi'an Jiaotong Liverpool University, Suzhou, Jiangsu 215123, PR China

ARTICLE INFO

Keywords:
$CuFeO_2$
Photoelectrochemical property
Water splitting

ABSTRACT

A Fe_2O_3 wrapped $CuFeO_2$ layer structure was fabricated on ITO glass by electrophoretic deposition and sol-gel methods at 400 °C. Such low fabrication temperature avoids the damage of ITO glass's transparency and conductivity. The $FeCl_3$ gel penetrated through the $CuFeO_2$ layer enhanced the connection and conductivity between $CuFeO_2$ particles and $CuFeO_2$/ITO glass interface. Pt particles were decorated on the surface by a photoreduction method to improve the PEC performance. The inserted Fe_2O_3 thin layer between the $CuFeO_2$ layer and Pt particles also worked as a buffer layer, which removed the upward barrier at the interface and improved the PEC activity.

1. Introduction

Semiconductor photoelectrodes have attracted much attention in relation to renewable energy technology for harvesting and conversion of solar light to hydrogen by water splitting reactions. Metal oxides with long-term stability in aqueous electrolytes and abundant reserves have been well-studied as the most attractive candidates for semiconductor photoelectrodes [1]. However, most of the metal oxide photoelectrodes are *n*-type with conduction band edges more positive than the redox potential of hydrogen reduction. They can only be used as photoanodes and are not suitable for hydrogen production. Research on cost-effective p-type oxide-based photocathodes is quite sparse. Recently, the research interest on p-type $CuFeO_2$ is growing as it possesses high stability in aqueous environment, visible light absorption and suitable band structure, which suggests the capability to develop a highly efficient photocathode for the reduction of water to hydrogen. As the most attractive front photoelectrode materials, intensive efforts have been devoted to developing $CuFeO_2$ photoelectrode in multiple-absorber-based tandem photoelectrodes to achieve high solar-to-hydrogen (STH) efficiency [2]. A few different fabrication methods have been reported to produce $CuFeO_2$ photocatalyst, such as electrochemical deposition [3], solid-state synthesis [4], sol-gel method [5] and microwave treatment was also used [6]. In order to achieve good conductivity between the $CuFeO_2$ film photoelectrode and substrate, annealing is essential, with the annealing temperature usually between 700 °C and 1000 °C, lasting for a couple of days [2,7,8]. For the most commonly used transparent conductive substrates, like ITO or FTO glass, such high temperature is harmful for their transparency and conductivity. It was reported that the $CuFeO_2$ film photoelectrodes can be destroyed resulting from the breakdown of FTO glass substrate above 700 °C annealing treatment [9].

In this study, we try to fabricate a Fe_2O_3 wrapped $CuFeO_2$ film photoelectrode on ITO glass substrate by alternately using electrophoretic deposition (EPD) and sol-gel method at 400 °C. Fe_2O_3 was used to enhance the connection of $CuFeO_2$ particles and the conductivity between $CuFeO_2$ particle layer and ITO glass without bring in impurity elements. The Fe_2O_3 also acted as a buffer layer on top of $CuFeO_2$ particle layer and formed a smooth surface for Pt catalyst particle decoration. This inserted Fe_2O_3 buffer layer between $CuFeO_2$ and Pt particles inhibited the formation of $CuFeO_2$/Pt Schottky upward barrier and made the photo-generated carriers separate efficiently in the electrode. A photocathodic current density of $-274\ \mu A/cm^2$ at 0 V *vs.* Ag/AgCl and an onset potential of 0.87 V *vs.* Ag/AgCl were obtained under $100\ mW/cm^2$ Xe lamp illumination. The photocathode shows high stability in aqueous electrolyte after 5 h PEC continuous testing and high faradic efficiency for hydrogen production.

2. Experimental

The Pt decorated Fe_2O_3 wrapped $CuFeO_2$ photoelectrode was

* Corresponding authors.
E-mail address: xiaorongcheng@126.com (X. Cheng).

https://doi.org/10.1016/j.chemphys.2018.08.009
Received 9 May 2018; Accepted 6 August 2018
Available online 10 August 2018

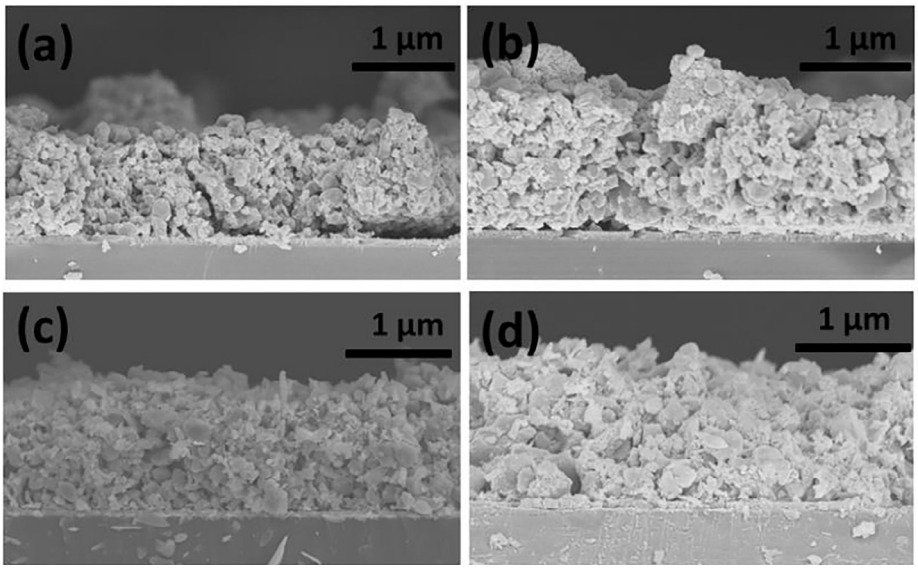

Fig. 1. Cross-sectional SEM images of (a) $CuFeO_2$ deposited on ITO glass substrate by EPD method (CFO-0), (b) CFO-1, (c) CFO-3 and (d) CFO-5.

fabricated by alternately using EPD and sol-gel methods. In a typical procedure, the $CuFeO_2$ powder was firstly prepared by calcination method at 1100 °C under Ar atmosphere as described in reference [8], and then deposited on ITO glass substrate by EPD method. The $CuFeO_2$ particles layer was then wrapped intimately by spin-coating $FeCl_3$ gel on the top 5 times and annealed at 400 °C for 2 h in air. Finally, the Pt catalyst particles were deposited on the surface by photochemical reduction (for more detailed procedures, see Supporting Information).

3. Results and discussion

Fig. 1a shows the loosely stacked $CuFeO_2$ particle layer deposited on ITO glass by an EPD method. Since the $CuFeO_2$ particles were only attracted to each other by weak electrical field forces and the 400 °C annealing process was not sufficient for re-crystallization of $CuFeO_2$ particles, the porous structure and irregular particle sizes we can see is reasonable. In addition, the $CuFeO_2$ particle layer also loosely contacted with the ITO glass substrate. An obvious gap was formed at the interface of $CuFeO_2$ particle layer and ITO glass. This poor connection among $CuFeO_2$ particles and poor conductivity between $CuFeO_2$ layer and ITO glass leads to the fragility of the photoelectrode in aqueous electrolyte. After one time of $FeCl_3$ gel spin-coating and annealing, the Fe_2O_3 filled in the voids among $CuFeO_2$ particles partially, as demonstrated in Fig. 1b. With the increasing of spin-coating times, the $FeCl_3$ gel permeation improved the connection among $CuFeO_2$ particles obviously and no obvious gap can be observed at the $CuFeO_2$ layer and ITO glass, as we can see in Fig. 1c and d.

The $FeCl_3$ gel spin-coating and annealing process can also change the surface morphology of samples. The CFO-0 sample shows a porous and uninformed surface morphology as we can see in Fig. 2a. The interparticle connection happens due to the $FeCl_3$ gel penetrating from the top of $CuFeO_2$ particle layer, which fills the surface voids and makes a close contact between the $CuFeO_2$ particles as shown in Fig. 2b and c. After 5 times of $FeCl_3$ gel spin-coating and annealing, a quite compact and smooth surface can be observed in Fig. 2d. Obviously, the surface morphology improved with the increasing of $FeCl_3$ gel spin-coating times. While 5 times is the optimal, after 6 times of spin-coating the surface of sample CFO-6 becomes cracked as shown in Fig. S1. This cracked surface structure impeded the stability of photoelectrode in aqueous electrolyte. The XRD pattern of the CFO-5 photoelectrode was measured and presented in Fig. S2, which shows the obvious diffraction peaks of well-crystallized $CuFeO_2$ and α-Fe_2O_3 in good agreement with the standard JCPDS cards NO.01-075-2146 and 01-085-0599. And the energy dispersive spectrometer (EDS) analysis for the cross section of the CFO-5 photoelectrode is also performed and presented in Fig. S3. Cu and Fe elements are dispersed throughout the film uniformly and the element content of Fe is a little bit higher than that of Cu. Considering these two element contents should be equal in pure $CuFeO_2$, it is reasonable to draw the conclusion that the Fe_2O_3 wraps the $CuFeO_2$ particles in the whole CFO-5 photoelectrode which leads to the higher Fe element content as shown in Fig. S3. There is no obvious Fe_2O_3 surface layer observable in Fig. 1d, with Fe_2O_3 uniformly distributed through the CFO-5 photoelectrode. Based on the above analysis, we draw the schematic model of CFO-5 photoelectrode as shown in Fig. S4. Notice here the Fe_2O_3 formed a thin buffer layer on the $CuFeO_2$ particle layer not a thick film. As the best performing catalyst for hydrogen evolved reaction (HER), Pt catalyst particles decoration has been proven to be effective to improve the PEC performance of the photoelectrodes. Here we fabricate the Pt catalyst particles on the surface of CFO-5 photoelectrode by photoreduction method (noted as CFO-5-Pt). The Pt particles are highly dispersed on the CFO-5-Pt surface with diameters of around 30 nm, as shown in SEM image of Fig. S5a. The EDS analysis of CFO-5-Pt surface in Fig. S5b further confirmed the uniform distribution of the Pt particles.

In Fig. 3a, we present the J–t curves of different photoelectrodes. There is no obvious photocurrent observed for CFO-0 and CFO-1 photoelectrodes. The CFO-3 photoelectrode exhibits a quite low photocurrent, which is due to the poor connection among $CuFeO_2$ particles and $CuFeO_2$/ITO glass interface, as we observed in Fig. 1. As for the CFO-5 photoelectrode, an obviously increased photocurrent, about $-95\ \mu A/cm^2$, is observed, indicating that the Fe_2O_3 wrapped structure is crucial to the separation and transport of photo-generated electron–hole pairs. The photocurrent can be further enhanced to $-274\ \mu A/cm^2$, after the Pt particles were decorated. Fig. 3b compares the J–V curves for CFO-5 photoelectrode before and after Pt particles decoration: the onset potentials (V_{op}) are 0.65 V and 0.87 V *vs.* Ag/AgCl, respectively. Here we define V_{op} as the point where the cathodic photocurrent appears on J–V curves. Thus, the Pt particles decoration enhanced the V_{op} of the photoelectrode significantly, consistent with the enhancement of the photocurrent. Here, the dark photocurrent was not zero but changed with the applied potential. This phenomenon is very common in J-V testing which can be explained by the back reaction of conduction band electrons with holes trapped at the photoelectrode surface [10]. Electrochemical impedance spectroscopy (EIS) measurements were carried out to better understand the PEC performance of CFO-5 photoelectrode before and after Pt particles decoration.

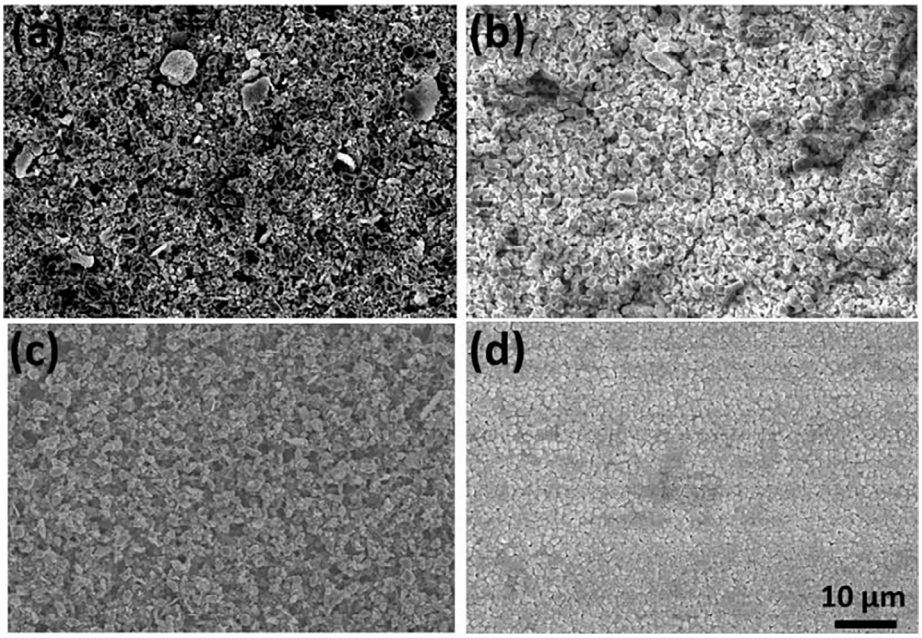

Fig. 2. Top-down SEM images of (a) CFO-0, (b) CFO-1, (c) CFO-3 and (d) CFO-5.

The Nyquist impedance plot of two photoelectrodes show semicircles as presented in Fig. 3c. The semicircles of high frequency range on the left are nearly the same, indicating that they are originated from the ITO/CFO interface. The second semicircles of low frequency range on the right change obviously after the decoration of Pt, indicating they are related to the front photoelectrode/electrolyte interface. As reported, the EIS data can be fitted to the different equivalent circuits [11]. The charge transfer resistance at ITO/CFO interface (R_1) indicated the coupling between the CFO and the ITO substrate. For CFO-5 photoelectrode before and after Pt decoration, R_1 are all around 261 Ω illustrated the Pt decoration on surface do not change the back ITO/CFO contact resistance. However, the total charge transfer resistance $R_4 = R_2 + R_3$ across the front photoelectrode/electrolyte interface changes significantly. R_4 reduces from 8654 Ω (R_2 equal to pure resistance at CFO/electrolyte interface in CFO-5 photoelectrode) to 4767 Ω (here R_2 represents resistance from CFO to Pt, R_3 represents resistance from Pt to electrolyte in CFO-5-Pt photoelectrode). Obviously, Pt decoration leads to the smaller diameters of the second circles, which correspond to smaller resistances for charge transfer at the photoelectrode/electrolyte interface and results in the improved

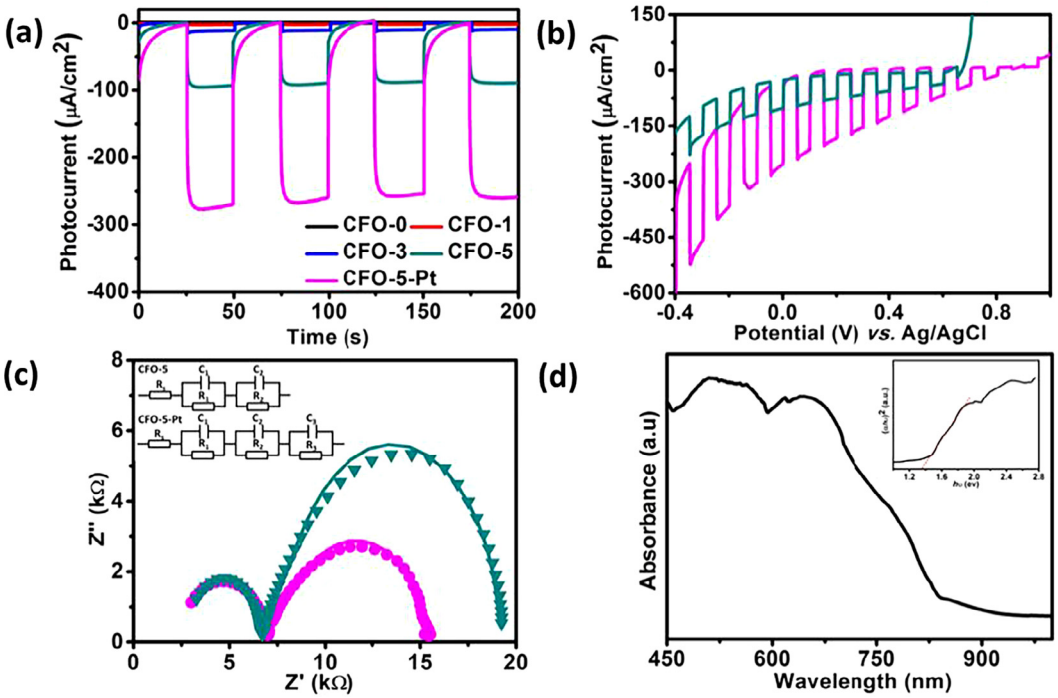

Fig. 3. (a) J–t and (b) J–V curves of different photoelectrodes, (c) EIS spectra and the solid traces correspond to the fitting curves of CFO-5 photoelectrode before and after Pt particles decoration, the insert is equivalent circuits and (d) UV–Vis absorption spectra of the CFO-5-Pt photoelectrode, the inset is the $(\alpha h\upsilon)^2 - (h\upsilon)$ plot.

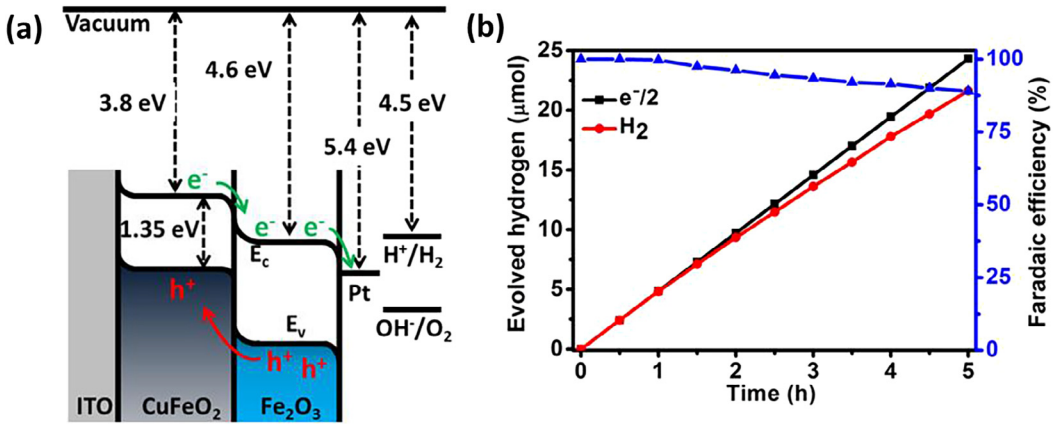

Fig. 4. (a) Energy band structure of CFO-5-Pt photoelectrode and (b) hydrogen production *vs.* time and Faradic efficiency curves of the CFO-5-Pt photoelectrode. The nearly straight line is the theoretical values of hydrogen production calculated based on the electrons passing through the circuit.

PEC activity [12]. Fig. 3d is the UV–Vis absorption spectra of the CFO-5-Pt photoelectrode with a broad absorption below 830 nm. The corresponding energy band gap was estimated to be 1.35 eV from the inset $(\alpha h\upsilon)^2 - (h\upsilon)$ plot, which is in agreement with reference [13], indicates that CFO-5-Pt photoelectrode can absorb considerable amount of visible light, implying its potential application as visible light driven photocathode. Table S1 in Supporting information compared CFO-5-Pt photoelectrode with other reported p-type semiconductor photocathodes. As we can see, the CFO-5-Pt photoelectrode show good PEC performance.

$CuFeO_2$ has a suitable conduction band position for photoreducing water to hydrogen, and the Pt particles were proved to be one of the best HER catalysts [2].The work function of Pt (5.64 eV) is much bigger than most of noble metal and $CuFeO_2$ [2]: as a result, an upward barrier will form at the $CuFeO_2$/Pt interface if the Pt particles were decorated on $CuFeO_2$ surface directly. This barrier will impede the photo-generated electrons moving out from the photoelectrode surface to the electrolyte. Fe_2O_3 is an *n*-type semiconductor with good energy band matching with Pt [14,15]. Therefore, after the Fe_2O_3 buffer layer was inserted into the $CuFeO_2$/Pt interface, the upward barrier was removed as illustrated in Fig. 4a. In addition, tunneling was also considered to be happening at the Fe_2O_3/Pt interface, since the Fe_2O_3 is very thin and highly conductive. As a result, the inserting of a Fe_2O_3 buffer layer removes the upward barrier and thus improves PEC activity. In addition to high efficiency, stability in aqueous electrolyte is also important for photoelectrode. We performed the long time stability test for CFO-5-Pt photoelectrode: for the good stability of Fe_2O_3 in electrolyte, a sustained photocurrent maintained at $-256\,\mu A/cm^2$ was observed for up to 5 h continuous PEC reaction, as shown in Fig. S6. We believe that the Fe_2O_3 wrapped $CuFeO_2$ and as buffer layer structure significantly enhanced the attachment of $CuFeO_2$ particle layer, resulting in improved PEC stability. The time course of hydrogen production and water splitting Faradic efficiency of CFO-5-Pt photoelectrode were measured and shown in Fig. 4b. The water splitting reaction was conducted in 0.1 M Na_2SO_4 electrolyte solution with an Ag/AgCl reference electrode and a Pt mesh counter electrode. A $100\,mW/cm^2$ Xe lamp as light source and no bias was added between CFO-5-Pt photoelectrode and Pt electrode. After the beginning of water splitting reaction, hydrogen and oxygen bubbles were observed on the surface of CFO-5-Pt photoelectrode and Pt mesh respectively. The evolved hydrogen gas was collected and measured by gas chromatography and the photocurrent was recorded to calculate the Faradic efficiency for hydrogen production. The Faradic efficiency of hydrogen evolution was maintained above 87% over the 5 h continuous water splitting reaction. The Faradic efficiency was less than 100%, probably due to the unwanted backward reaction between hydrogen and oxygen [16].

4. Conclusions

In summary, we report a simple electrophoretic deposition and sol-gel route to fabricate a Fe_2O_3 wrapped $CuFeO_2$ layer structure photocathode on ITO glass substrate at 400 °C. The $FeCl_3$ gel fills up the voids among $CuFeO_2$ particles and enhanced the connection between $CuFeO_2$ particles layer and ITO glass substrate after annealing. The Fe_2O_3 also acts as a buffer layer at the $CuFeO_2$/Pt interface, inhibiting the formation of an upward barrier. As a result, a photocathodic current density of $-274\,\mu A/cm^2$ at 0 V *vs.* Ag/AgCl and an onset potential of 0.87 V *vs.* Ag/AgClwere obtained in 0.1 M Na_2SO_4 electrolyte under $100\,mW/cm^2$ Xe lamp illumination. The photocathode also shows high Faradic efficiency and stability after 5 h continuous water splitting testing. This study provides a new route to prepare $CuFeO_2$ as film photocathode on transparent substrate under low temperature and we propose that this work makes available a new pathway to the fabrication of delafossite compounds photoelectrodes under low temperature.

Acknowledgments

This work was supported by Suzhou Institute of Industrial Technology Research Fund (Grant No. SGYKJ201705 and 2017kyqd010), Xi'an Jiaotong Liverpool University Research Development Fund and National Natural Science Foundation of China (Grant No. 21650110446), Natural Science Foundation of Jiangsu Province (No. BK20160352).

Appendix A. Supplementary data

Supplementary data associated with this article can be found, in the online version, at https://doi.org/10.1016/j.chemphys.2018.08.009.

References

[1] M. Woodhouse, B.A. Parkinson, Chem. Soc. Rev. 38 (2009) 197–210.
[2] M.S. Prévot, X.A. Jeanbourquin, W.S. Bourée, F. Abdi, D. Friedrich, R. van de Krol, N. Guijarro, F. Le Formal, K. Sivula, Chem. Mater. 29 (2017) 4952–4962.
[3] U. Kang, S.K. Choi, D.J. Ham, S.M. Ji, W. Choi, D.S. Han, A. Abdel-Wahab, H. Park, Energy Environ. Sci. 8 (2015) 2638–2643.
[4] A. Wuttig, J.W. Krizan, J. Gu, J.J. Frick, R.J. Cava, A.B. Bocarsly, J. Mater. Chem. A 5 (2017) 165–171.
[5] M.S. Prévot, N. Guijarro, K. Sivula, ChemSusChem 8 (2015) 1359–1367.
[6] Y.J. Jang, Y.B. Park, H.E. Kim, Y.H. Choi, S.H. Choi, J.S. Lee, Chem. Mater. 28 (2016) 6054–6061.
[7] Y.J. Oh, W.S. Yang, J.M. Kim, S.H. Jeong, J.H. Moon, ACS Appl. Mater. Interfaces 9 (2017) 14078–14087.
[8] J.W. Lekse, M.K. Underwood, J.P. Lewis, C. Matranga, J. Phys. Chem. C 16 (2012) 1865–1872.
[9] A. Annamalai, A. Subramanian, U. Kang, H. Park, S.H. Choi, J.S. Jang, J. Phys. Chem. C 119 (2015) 3810–3817.

[10] A. Hagfeldt, H. Lindström, S. Södergren, S. Lindquist, J. Electroanal. Chem. 381 (1995) 39–46.
[11] Y.L. Huang, W.S. Chang, C.N. Van, H.J. Liu, K.A. Tsai, J.W. Chen, H.H. Kuo, W.Y. Tzeng, Y.C. Chen, C.L. Wu, C.W. Luo, Y.J. Hsu, Y.H. Chu, Nanoscale 8 (2016) 15795–15801.
[12] T. Lopes, L. Andrade, H.A. Ribeiro, A. Mendes, Int. J. Hydrogen Energy 35 (2010) 11601–11608.
[13] Y. Jin, G. Chumanov, RSC Adv. 6 (2016) 26392–26397.
[14] G.M. Wang, Y.C. Ling, D.A. Wheeler, K.E.N. George, K. Horsley, C. Heske, J.Z. Zhang, Y. Li, Nano Lett. 11 (2011) 3503–3509.
[15] P. Kumar, P. Sharma, R. Shrivastav, S. Dass, V.R. Satsangi, Int. J. Hydrogen Energy 36 (2011) 2777–2784.
[16] E.S. Kim, N. Nishimaru, G. Magesh, J.Y. Kim, J.W. Jang, H. Jun, J. Kubota, K. Domen, J.S. Lee, J. Am. Chem. Soc. 135 (2013) 5375–5383.